# Autonomous reciprocating migration of an active material

Lin Ren[a], Meng Wang[a], Changwei Pan[a], Qingyu Gao[a,1], Yang Liu[a], and Irving R. Epstein[b,c,1]

[a]College of Chemical Engineering, China University of Mining and Technology, Xuzhou, 221008 Jiangsu, People's Republic of China; [b]Department of Chemistry, Brandeis University, Waltham, MA 02454-9110; and [c]Volen Center for Complex Systems, Brandeis University, Waltham, MA 02454-9110

Edited by Thomas E. Mallouk, The Pennsylvania State University, University Park, PA, and approved July 5, 2017 (received for review March 15, 2017)

**Periodic to-and-fro migration is a sophisticated mode of locomotion found in many forms of active matter in nature. Providing a general description of periodic migration is challenging, because many details of animal migration remain a mystery. We study periodic migration in a simpler system using a mechanistic model of a photosensitive, active material in which a stimulus-responsive polymer gel is propelled by chemical waves under the regulation of an illumination gradient sensed by the gel, which plays a role analogous to the environment in periodic animal migration. The reciprocating gel migration results from autonomous transitions between retrograde and direct wave locomotion modes arising from the gradient distribution of the illumination intensity. The local dynamics of the chemical waves modulates the asymmetry between push and pull forces to achieve repeated reorientation of the direction of locomotion. Materials that display similar intelligent, self-adaptive locomotion might be tailored for such functions as drug delivery or self-cleaning systems.**

active matter | Belousov–Zhabotinsky reaction | chemomechanical transduction | periodic migration

In a nonequilibrium state, an element of active matter may consume energy to generate motion (1–4). The movement can be either nondirectional or unidirectional (2) and depends on the asynchrony or synchrony of collective behaviors on a macroscopic level (3, 4). For the directional locomotion of matter, orientation may be achieved by exploiting the ability to sense a gradient of a stimulus in the environment (5) [e.g., biological locomotion toward or away from a positive gradient of illumination, concentration, or temperature; i.e., positive or negative phototaxis (6), chemotaxis (7), or thermotaxis (8), respectively]. This response plays an essential role in ensuring the survival of many organisms subjected to a heterogeneous distribution of resources or hazardous substances in their habitat (9). Furthermore, in nature, the locomotion of active matter is not simply unidirectional (2) but involves more advanced modes to adapt to the complexity and severity of the environment. Remarkable examples, most of which remain to be comprehensively understood (10, 11), include the periodic migration of animals (12, 13), cells (10, 14, 15), and biomacromolecules (16).

One striking example is the anadromous migration of salmon (13). The fish are born in high-latitude tributaries or lakes, swim into the ocean for temporary habitation, and ultimately, return as adult fish to their place of birth with remarkable precision for the purpose of spawning. This process plays a critical role in ecological balance by spatially transporting nutrients, such as nitrogen, contributing to the matter cycling of nutrients that are carried from the ocean to the land to feed the associated biocoenosis. Stimulus-gradient sensing plays a dominant role in guiding the fish through a nearly constant environment (13). Salmon direct their swimming toward or away from the specific migration area depending on aspects of their physiological state, such as age, nutrition, and climate (13). In other words, the directional dynamics of self-propelled entities interacts with the position-dependent environment to generate periodic locomotion; similar situations occur in the periodic locomotion of cells produced by spatial constraints (10, 15) and with swimming bacteria (17). However, fundamental questions remain. Can one give a general mechanistic description of periodic reciprocating migration, which is an obvious advance over its unidirectional counterpart? In the absence of the extremely complex machinery of the abovementioned living organisms, can analogous migratory behavior emerge?

Here, we investigate an artificial active matter system that undergoes periodic migration in a fixed, heterogeneously illuminated environment using a widely studied self-oscillating polymer gel that hosts the tris(bipyridine)ruthenium [Ru(bipy)]-catalyzed Belousov–Zhabotinsky reaction (BZR) (18–20). In this stimulus-responsive gel, the redox state of the catalyst undergoes periodic changes during the BZR oscillations, which generate autonomous swelling and deswelling of the gel. The Belousov–Zhabotinsky (BZ) waves and stimulus-responsive gel can be thought of as analogs of the nerve pulses and deformable muscles in animals, respectively (21). A chemomechanical model of the BZ gel, the gel lattice-spring model (gLSM), has been developed by Balazs and coworkers (22–24). The gLSM can capture large-scale shape changes and the locomotion of the gel (25). Moreover, the photosensitivity of the Ru(bipy) catalyst enables one to modify the locomotion direction by changing the pattern of illumination (26) to produce, for example, negative or positive phototaxis (27) or direct wave (DW) or retrograde wave (RW) locomotion (21) (i.e., movement in the same or the opposite direction that the "muscular" wave travels, respectively).

Although important progress has been made toward understanding the directional locomotion of gels driven by chemical waves (21, 26, 27), there are still challenges. Can one generate autonomous reciprocating locomotion of a photosensitive self-oscillating gel that mimics the dynamics of animal migration,

## Significance

We analyze the reciprocating locomotion of a photosensitive gel undergoing an oscillating chemical reaction in a temporally constant gradient illumination environment to examine whether periodic migration can arise as an adaptive response of a system's internal dynamics, analogous to biological functions like growth or breeding, to specific spatial variations in resource distribution, such as food, temperature, or light intensity, caused by geography or seasonal transition. Even in this relatively simple system, kinematic switching in the mode of locomotion under spatially varying illumination levels leads to reciprocating periodic motion, suggesting that such behavior may occur widely in organisms as a response to a variety of spatially distributed environmental stimuli to enhance their survival and reproduction.

Author contributions: L.R., Q.G., and I.R.E. designed research; L.R., M.W., C.P., Q.G., Y.L., and I.R.E. performed research; L.R., M.W., C.P., Q.G., Y.L., and I.R.E. analyzed data; and L.R., Q.G., and I.R.E. wrote the paper.

The authors declare no conflict of interest.

This article is a PNAS Direct Submission.

[1]To whom correspondence may be addressed. Email: gaoqy@cumt.edu.cn or epstein@brandeis.edu.

This article contains supporting information online at www.pnas.org/lookup/suppl/doi:10.1073/pnas.1704094114/-/DCSupplemental.

such as the anadromous migration of salmon? In nature, the variation of environmental parameters usually exhibits smooth geographic variation with a relatively small slope rather than step-like gradients. The slopes of geographic parameters, such as temperature and illumination, during bird migration are nearly constant along latitudes in spring and autumn, and the slopes of parameters, such as food, temperature, and salinity, during salmon migration vary only slightly along North American longitudes. Thus, study of a gel motor moving in a gradient illumination with finite slope may offer insight into the adaptive migration of animals. Nonautonomous reciprocating migration of such gels can be forced by externally adjusting illumination levels (21), but such studies cannot contribute to our understanding of the autonomous migration of animals in natural environments.

Two key components of periodic BZ migration have been identified. First, self-oscillating BZ gels or their analogs undergo directional movement (28) propelled by a force asymmetry between the push at the front and the pull at the back of a pulse wave or vice versa produced by the intrinsic dynamics of the reaction transport system independent of any nonuniform features of the environment. In Fig. S1, we illustrate how, with periodic boundary conditions (i.e., on a pseudo-1D ring), autonomously propagating pulse waves propel the gel to undergo directional locomotion because of this push–pull effect. Second, interaction between a BZ gel and any asymmetry in its environment produces a spatial gradient of stimulus intensity, which can result in a transition between oppositely directed modes of locomotion (i.e., RW and DW). Thus, it should be possible to control the autonomous periodic locomotion of an active material by combining these two phenomena. We shall see that periodic migration can be brought about by patterning the illumination to which the gel is exposed so as to modulate the structure of the pulse waves, altering the force asymmetry between the wave front and the wave back. We first explore the periodic migration of the gel in detail. Then, we characterize it using order parameters to analyze the chemical origins of the migration.

## Results

**Autonomous Reciprocating Migration of the Active Gel.** To investigate the autonomous motion of the gel under gradient illumination, we incorporate a two-variable photosensitive Oregonator model (27, 29), which describes both photopromotion and photoinhibition of the photosensitive BZR, into the gLSM. The BZ gel can sense nonuniform illumination through the nonmonotonic relationship between the imposed light intensity and the oscillation frequency of the Ru(bipy)-catalyzed BZR (21, 27, 30). Chemical waves in the gel propagate from a region of higher to lower frequency, and therefore, the wave with highest frequency determines the ultimate direction of wave travel in this heterogeneous oscillatory BZR medium (31–33). For the pattern of illumination in Fig. 1*A*, *Upper* (which corresponds to Fig. S2), the pulse waves always move toward areas of lower illumination intensity (i.e., the waves propagate from right to left) (Fig. 1 *E* and *F*). Depending on the parameters of the illumination pattern, we obtain simple RW locomotion, DW locomotion, or autonomous periodic migration of the gel (Fig. 1). In Fig. S3, we illustrate these three modes of gel locomotion in the $f$–$\alpha$ plane, where $f$ is the "stoichiometric factor" in the Oregonator model, which characterizes the organic chemistry of the BZ system, and $\alpha$ measures the slope of the illumination intensity gradient as shown in Fig. S2. Thus, the locomotion behavior depends on both the intrinsic chemistry and the external environment.

The time evolutions of the left grid point ($R_l$), center grid point ($R_c$), and right grid point ($R_r$) of the gel are shown in Fig. 1*A*, which displays autonomous periodic migration under temporally constant inhomogeneous illumination. A clearer exhibition of $R_c$ vs. time over one period of the migration is shown in Fig. 1*B*, where we identify four characteristic time intervals marked as one to four, which correspond to the RW phase, the transition from RW to DW locomotion, the DW phase, and the transition from DW to RW, respectively. Expanded views of these intervals are shown in Fig. 1*B*, *Insets*, showing that the net displacement of the grid point is a sum of reciprocating motions driven by successive chemical waves. For intervals one to four, the reciprocating motions of the gel are shown to be simple oscillations (Fig. 1*B*, *Inset 1*, $+x$ locomotion), irregular oscillations (Fig. 1*B*, *Insets 2 and 4*, transitions from one direction of locomotion to the other), or complex oscillations (Fig. 1*B*, *Inset 3*, $-x$ locomotion). Enlarged views of the gel locomotion in the RW and DW phases are shown in Fig. 1 *C* and *D*, where the gel moves opposite to or along the direction of wave propagation ($-x$ direction) as shown in Fig. 1 *E* and *F*, respectively. The simple pulse waves (Fig. 1*E*) and rippled waves (local backfiring) (Fig. 1*F*) correspond to the simple and complex oscillatory grid trajectories for the RW and DW locomotion shown in Fig. 1*B*, *Insets 1 and 3*, respectively.

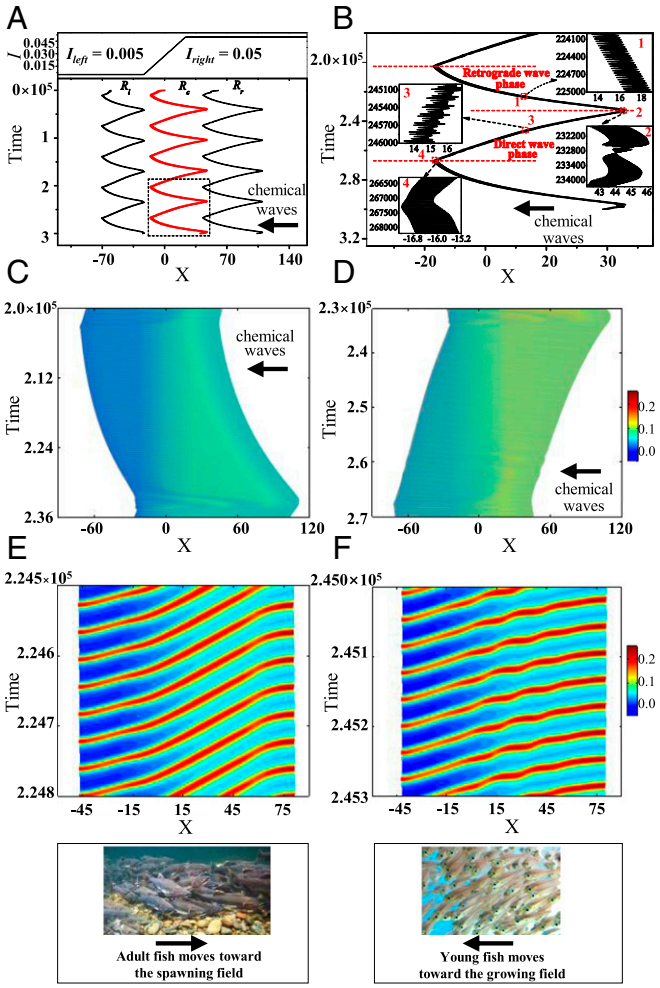


**Fig. 1.** Autonomous periodic migration of the gel and a fish analogy. (*A*) Motion of the gel grid points at the left boundary ($R_l$), the right boundary ($R_r$), and the gel center ($R_c$). *Upper* shows the illumination distribution, $\alpha$ = 0.05. (*B*) $R_c$ vs. time over one cycle of the migration. Intervals of RW and DW phases are marked. *Insets* are enlarged views of four characteristic intervals labeled one to four. *C* and *D* are spatiotemporal plots of gel locomotion over the RW and DW phases, respectively. Corresponding enlarged views show chemical wave propagation in *E* and *F*, respectively; each plot consists of 600 data points at 0.5$\tau$ intervals. Color denotes the value of variable *v*. *E*, *Lower* and *F*, *Lower* are pictures of salmon migration in the locomotion phase of returning to or departing from their birthplace. Movies S1 and S2 show autonomous periodic migration of the whole and a smaller gel fragment.

In general, interconversion of two different types of pulse waves results in transition between RW and DW locomotion of the gel.

The above observations suggest that the autonomous locomotion of the gel can be functionally decomposed into two facets. One is the gel locomotion, which is driven by the waves. The other is the interconversion between simple pulse waves and local backfiring ripple waves under the specific pattern of gradient illumination. To return to our animal analogy, the first aspect corresponds to locomotion propelled by muscle deformations controlled by nerve pulses, whereas the second results from the multiple physiological states of animals, such as newborn fish and adult fish, which are differentially sensitive to the spatiotemporal distribution of food, temperature, salinity, and other stimuli in the environment. These two features generate autonomous periodic migration (e.g., the anadromous migration of salmon populations), analogous to the autonomous periodic migration of the gel in our simulation. For example, adult fish swim back toward their birthplace, the spawning field, during the return phase of the migration. After spawning there, the newborn fish mature and then navigate to the sea (departing phase) for additional growth. One phenomenon connecting the two locomotion phases is spawning; the other is sexual maturation before returning to the river. Both scenarios involve substantial changes in the physiological state of the fish. Similarly, the chemical waves undergo major changes in regions 2 and 4, thus enabling them to reverse their direction of locomotion, resulting in periodic reciprocating migration.

**Wave Kinematics.** We can simplify our description of the propagating waves by identifying the point in each wave at which $v$, the concentration of oxidized catalyst, reaches its maximum and plotting these positions as a function of time (Fig. S4). These space–time plots can then be used to calculate both the local velocity $[V_l(x)]$ and the local curvature $[\kappa(x)]$ to characterize the wave. Details of this calculation can be found in *SI Text*. Fig. 2 shows spatiotemporal plots of $\kappa(x)$ and $1/V_l$ over one cycle of the migration. The yellow color in Fig. 2*A* corresponds to a smoothly propagating local wave, where the curvature is small. Such behavior is seen in the RW phase in Fig. 1*B*, *Inset 1* and *C*. At the end of this phase, the locally increasing value of $\kappa(x)$ signals that the wave's structure undergoes spatiotemporal distortion (i.e., the simple pulse wave loses stability) as shown in the enlarged view in Fig. 2*B* and Fig. 1*B*, *Inset 2*. The local velocity (Fig. 2*D*; an enlarged view is in Fig. 2*E*) helps us to identify this instability as a local backfiring instability (34); that is, the wave loses stability via the generation of new local waves that travel opposite to the direction of the dominant wave. In Fig. 2*E*, the red regions in the plot denote local waves traveling in the $+x$ direction, whereas the dominant wave propagates along $-x$. Next, the DW phase begins as the locomotion of the gel reverses direction and the local curvature and wave velocity fluctuate as manifested in the rippling waves seen in Fig. 1*F* and shown in Fig. 2 *D* and *E* as fluctuations of $1/V_l(x)$. These features indicate a cyclic undulatory velocity of wave propagation in the DW phase. At the end of the DW phase, fluctuation of $\kappa(x)$ disappears via a reverse backfiring instability (Fig. 2*C*) to open the next RW phase of the migration.

The above analysis outlines the essential features of the transitions that the waves undergo over one cycle of migration. Another property of the wave can be extracted from the data shown in Fig. 2*D* regarding the mean velocity of wave propagation. Keeping in mind that the figure shows the reciprocal of the velocity and that larger absolute values (deeper blue in Fig. 2*D*) correspond to slower waves, we observe that, on average, waves in the RW phase propagate more slowly than waves in the DW phase. The averages, $\overline{V_l}$, are about 2.0 and −1.3 in the DW and RW phases, respectively, as estimated from the data in Fig. 2*D*.

To concisely describe the global features of the wave kinetics over the gel, we define two order parameters, $\beta$ and $V_w$, by spatially integrating $\kappa(x)$ and $V_l(x)$, respectively, over the length of the gel, because the net locomotion of the gel is determined by the collective propulsion effect of all of the local waves. $\beta$ is given by

$$\beta = \sqrt{\sum_{i=1}^{N} \frac{(\kappa(i) - \overline{\kappa})^2}{N}}. \quad [1]$$

Thus, $\beta$ is the mean squared error of $\kappa(x)$ over all grid points of the gel. It increases with both the strength and the number of distorted structures in a wave. The summation is over the $N$ grid elements: 100 in our simulation. The other order parameter is $V_w$, the mean velocity of a propagating wave across the gel. In Fig. 3*A*, we depict how both order parameters vary along the position of the gel's center over approximately four cycles of migration. This portrait in the $V_w$–$\beta$–$X_{gelcenter}$ space shows the limit cycle character of the motion. Most of the trajectory consists of the RW and DW phases (marked with green dashed and red dotted lines, respectively, in Fig. 3*A*), where the system is in a relatively stable state. The two phases clearly have quite different values of $\beta$ and $V_w$. They are linked by transitions, marked as point one and point two, respectively.

The total migration process can thus be described as follows. Initially, the gel undergoes retrograde motion along the $+x$ direction toward higher light intensity. When it reaches a region of sufficient light intensity, the simple pulse waves lose stability (as shown by the large increase in $\beta$ near point one), and the system transitions to the DW phase with both a higher wave velocity and a reversal of the movement direction of the gel (now along the $-x$ direction). A similar transition occurs at the end of the DW phase when the gel enters the low-light intensity region. The local backfiring waves lose stability near point two and then recover to RW ($+x$ direction) locomotion with lower wave velocity, and the cycle begins again. Note that the kinetic state of the system is maintained over relatively long periods during each phase but undergoes rapid changes in the conversion between phases.

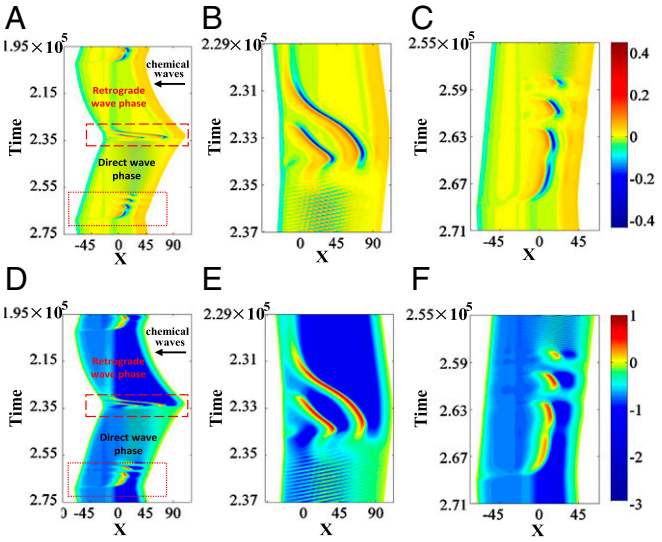


**Fig. 2.** Spatiotemporal plots of kinematic parameters of a chemical wave ($v$) during one cycle of the gel's periodic migration. (*A*–*C*) Spatiotemporal plots of local curvature ($\kappa$). *B* and *C* are locally enlarged views of *A* for rectangular regions with dashed and dotted boundaries, respectively. *D*–*F* are spatiotemporal plots of the reciprocal of local velocity ($1/V_l$) of chemical wave propagation. *E* and *F* are enlarged views of *D* for dashed and dotted rectangular regions, respectively.

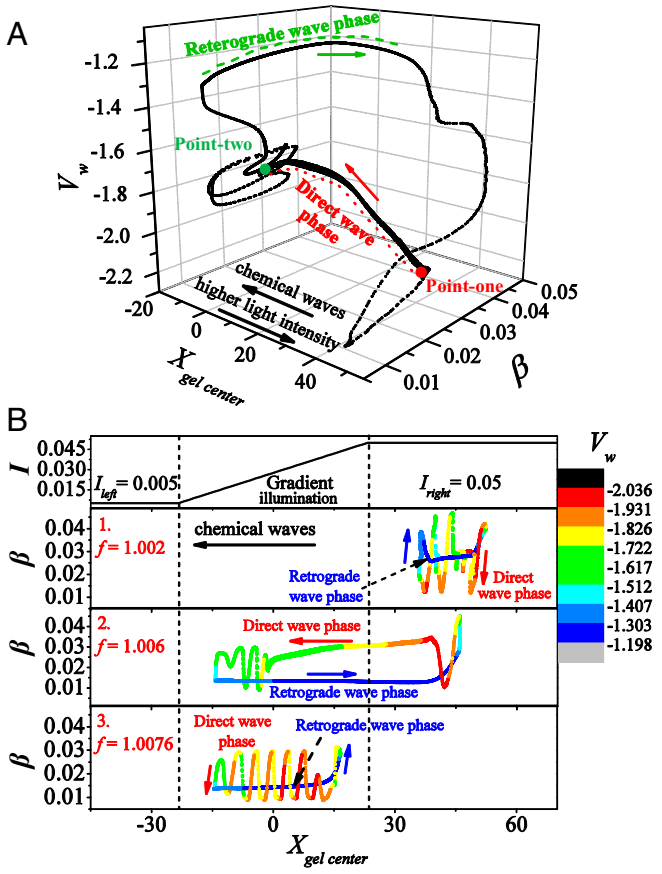


**Fig. 3.** Dynamic attractor of the autonomous periodic locomotion. (*A*) $V_w$–$\beta$–$X_{gelcenter}$ space at $f$ = 1.006. (*B*) $\beta$–$X_{gelcenter}$ plane at three values of $f$ with color-indicated $V_w$ values: $f$ = 1.002 (curve 1), $f$ = 1.006 (curve 2), and $f$ = 1.0076 (curve 3). *B*, *Upper* shows illumination distribution. $\alpha$ = 0.055.

We can use our order parameters to examine how the behavior of the system changes as its chemistry, characterized by the parameter $f$, is varied. Fig. 3*B* shows three scenarios of migration (Fig. 3*B*, curves 1–3) at $f$ = 1.0076, 1.006, and 1.002, respectively. For ease of comparison, we represent the values of $V_w$ as colors on the three migration trajectories in the $\beta$–$X_{gelcenter}$ plane along with the illumination distribution shown in Fig. 3*B*, *Upper*. The three scenarios illustrate two different kinetic states of wave propagation: waves propagating in the RW and DW phases with low and high degrees, respectively, of distortion in the wave propagation. Curves 1 and 3 indicate that, depending on the chemistry of the system, the gel migration can be centered in either the low or the high illumination region, although with relatively small migration amplitude. Regardless of where the migration occurs, $\beta$ increases just before each transition, which indicates an illumination-induced instability of the simple pulse waves. In all cases, the absolute velocity of wave propagation is lower (~1.3) in the RW phase and higher (>1.6) in the DW phase. Clearly, the velocity of wave propagation plays a key role in the transition between locomotion phases.

**Gel Kinematics.** Two questions require additional discussion. Why do the waves lose stability under the differential illumination, and how does $V_w$ affect the illumination-induced instability that generates the two kinetic states that alternately drive the gel in opposite directions? To answer these questions, we examine the kinematic details of the propulsion of the gel by the pulse waves. Fig. 4 shows several features of the gel locomotion in the RW and DW phases. $V_g$ denotes the mean velocity of the gel's center, which because of the synchronous dynamics of the gel system, is a suitable measure of the locomotion velocity of the gel. Comparing the gel (Fig. 4*A*, *Second Row*) and average pulse wave (Fig. 4*A*, *Third Row*) velocities with the motion of the gel center (Fig. 4*A*) over a single cycle of migration, we observe that, in the DW phase, $V_g$ is negative and $|V_w|$ is high, whereas in the RW phase, $V_g$ is positive and $|V_w|$ is low. Strikingly, the value of $V_w$ at both the RW to DW and the DW to RW transitions is the same, about −1.45, which suggests that $V_w$ plays a key role in the locomotion transition.

Additional insight into how $V_w$ affects the gel locomotion can be obtained by a kinematic analysis of $V_g$. In the theory of 1D BZ gels, $V_g$ is the ratio between the time integral of the velocity of the polymer network, $V_p$, over one motion cycle and the period of the cycle (one wave). $V_p$ can be written as (23)

$$V_p = \frac{\nabla\sigma}{\zeta'(\phi)}, \qquad [2]$$

where $\nabla\sigma = \nabla(\pi_{osm} - \sigma_{el}^{1D})$, $\zeta'(\phi) = \Lambda_0^{-1}(\phi/\phi_0)^{3/2}/(1-\phi_0)$, $\nabla\sigma$ is the stress gradient, and $\zeta'(\phi)$ is the apparent friction coefficient. $\sigma_{el}^{1D}$ is the 1D elastic force, $\pi_{osm}$ is the osmotic pressure, $\Lambda_0$ is a dimensionless kinetic coefficient, and $\phi_0$ denotes the undeformed

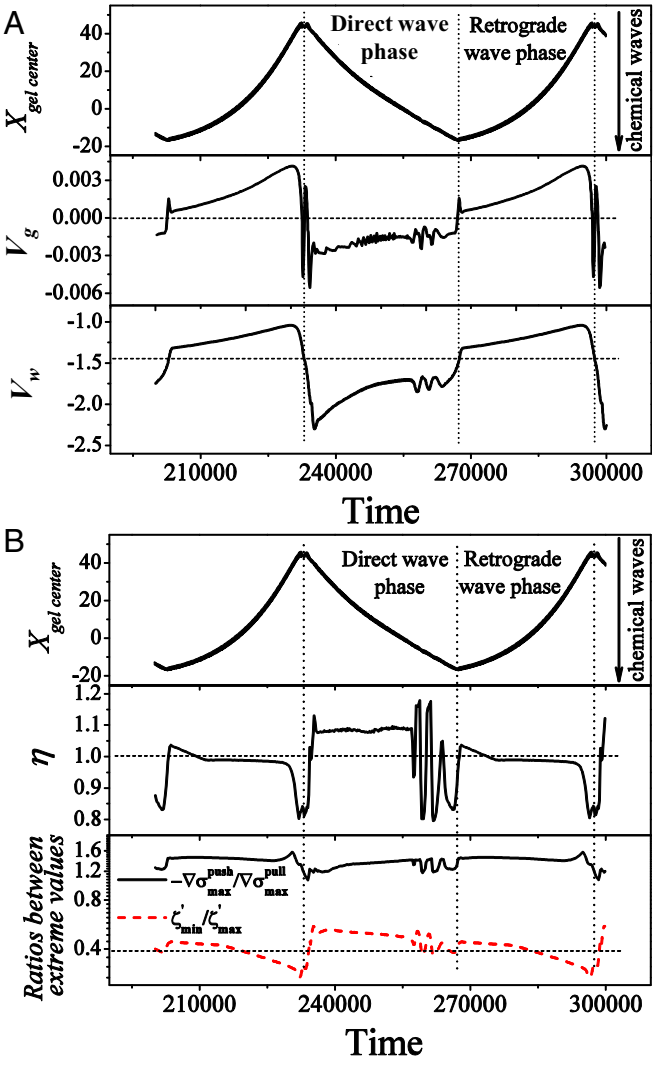


**Fig. 4.** Time series of kinematic parameters. (*A*) $V_g$ and $V_w$ vs. time. (*B*) $\eta$, $-\nabla\sigma|^{push}_{max}/|\nabla\sigma|^{pull}_{max}$, and $\zeta'_{min}(\phi)/\zeta'_{max}(\phi)$ vs. time.

polymer volume fraction. For a gel driven by chemical waves, each period of chemical wave propagation is composed of a wave front and a wave back, which successively push and pull the local gel, respectively (21). Movement of the gel under successive push and pull activity composes one motion cycle. The competition between the oppositely directed time integrals of $V_p$ over the push and pull phases in a motion cycle determines the net displacement of the gel during that cycle (i.e., whether the gel experiences DW or RW locomotion) (21). The push effect benefits DWs, whereas the pull effect favors RWs. To concisely express this competition, we characterize it using the extreme values of $V_p$ in the push and pull phases of each wave to approximately replace the time integrals of $V_p$ in each phase. We choose $\gamma = 0.75398$ to satisfy the following equation:

$$-\sum_T V_{p\ max}^{push} = \gamma \sum_T V_{p\ max}^{pull}. \quad [3]$$

Eq. **3** expresses the fact that, for a full cycle of periodic migration with period $T$, the time integrals, which are proportional to $V_{p\ max}^{push}$ and $V_{p\ max}^{pull}$ summed over all of the waves that make up the cycle, must have the same magnitude, because the net displacement during one period of the migration is zero. Then, we define a parameter $\eta$ to describe the push–pull competition during each wave, which can be written as

$$\eta = \frac{-V_{p\ max}^{push}}{\left(\gamma V_{p\ max}^{pull}\right)}. \quad [4]$$

Therefore, as shown in Fig. 4*B*, when $\eta > 1$, the push effect is dominant, and the gel undergoes DW locomotion; for $\eta < 1$, the pull effect is dominant, resulting in RW locomotion. The time series shows the cyclical variation of $\eta$ around 1.0, which accounts for the periodic reciprocating migration.

The following analysis shows that the oscillation of $\eta$ over a migration cycle (Fig. 4*B*) arises from the variation of the dynamic characteristics of the gel [$\nabla\sigma_{extreme}$ and $\zeta'_{extreme}(\phi)$] and is ultimately the result of changes in the kinetics of the wave. The third row in Fig. 4*B* shows the ratios $-|\nabla\sigma|_{max}^{push}/|\nabla\sigma|_{max}^{pull}$ and $\zeta'_{min}(\phi)/\zeta'_{max}(\phi)$. According to Eq. **2** and our previous work (21), $V_{p\ max}^{push} = \nabla\sigma_{max}^{push}/\zeta'_{max}(\phi)$, and $V_{p\ max}^{pull} = \nabla\sigma_{max}^{pull}/\zeta'_{min}(\phi)$. Thus, we conclude that the periodic change of $\eta$ is primarily the result of the variation in $\zeta'_{min}(\phi)/\zeta'_{max}(\phi)$, because its value in the DW phase is significantly different from that in the RW phase as indicated by the red dashed line in Fig. 4*B*. In contrast, the other dynamic term, $\nabla\sigma_{max}^{push}/\nabla\sigma_{max}^{pull}$, changes only minimally between the two phases. Because the apparent friction coefficient $\zeta'(\phi)$ is a monotonic function of the volume fraction of the gel ($\phi$), a ratio $\zeta'_{min}(\phi)/\zeta'_{max}(\phi)$ less than one indicates a larger ratio between the deswelling and swelling of the gel [deswelling–swelling (DS) ratio: $\phi_{max}/\phi_{min}$]. That is, the DS ratio has a higher value in the RW phase than in the DW phase, which is the key factor in producing the migration. Finally, we discuss the chemical origin of the variation of the DS ratio. More details can be found in Fig. S5. The analysis shows that the variation of the propagation velocity of the wave generates changes in the value of the kinetic term, $\nabla^2 v$, which accounts for the different DS ratios of the gel in the RW and DW phases.

**Dynamical Origin of Autonomous Reciprocating Migration.** The illumination-induced dynamical instability of the chemical waves (i.e., the transition between simple pulse waves and local backfiring pulse waves) can be analyzed in terms of the local kinetics, because the pulse waves are generated from the diffusion of local oscillations over the gel. We have looked at both the local oscillations at the gel center and the oscillations at different positions along the gel (Fig. S6) during periodic migration. Fig. 5*A* shows $v_{max}$ for oscillations at the gel center as a function of $X_{gelcenter}$, which provides insight into the spatiotemporal structure of the complete gel because of the synchronous system dynamics. From $t$ = 202,000–232,000, the gel is in the RW phase, and the smooth behavior of $v_{maxcenter}$ vs. $X_{gelcenter}$ (black curve in Fig. 5*A*) is associated with the regular local oscillations in Fig. 5*B*. In the high-illumination region (i.e., at the end of the RW phase), the oscillations become unstable, resulting in the reversal of direction of the gel locomotion. The gel quickly enters the DW phase, and $v_{max}$ shows complex oscillations (Fig. 5*C*), exhibiting local backfiring pulse waves along the gel as seen in the red curve in Fig. 5*A*. Ultimately, the local dynamics return to simple oscillations (the RW phase). Additional details can be found in Fig. S6, which displays the dynamics at different positions of the gel with the gel center fixed.

These results show the relationships between local dynamics, wave structure, and locomotion phase. Two key features can be identified. One is the illumination-induced instability of the simple oscillations caused by the photochemical reaction, which generates bromide ion, an inhibitor of the oscillation (30). The second is the bistable (hysteretic) transition between simple and complex oscillations. That is, the position of the transition point from simple to complex oscillations is not the same as the reverse transition point from complex to simple oscillations. This hysteretic transition provides the dynamic impetus for the autonomous periodic migration of the gel under light gradients within a specific slope range (Fig. S3), which differs fundamentally from the phenomenon of nonautonomous transition between locomotion modes driven by adjusting the external illumination (21) under a step-like gradient of light, where external intervention is required to reverse the direction of locomotion.

## Discussion

We have designed an autonomous photosensitive worm-like motor in an effort to understand the underlying dynamics of some biological periodic migrations. The active material, a BZ oscillating gel, was used under gradient illumination to convert RW locomotion to DW locomotion and vice versa at low and high light intensities, respectively, resulting in autonomous bidirectional locomotion. This cyclic behavior is driven by changes in the BZR spatiotemporal waves, which are dominated by the local dynamics, as the gel moves between low and high light intensities. Smaller fragments of gel than the one discussed above can migrate over distances of multiple body lengths (an

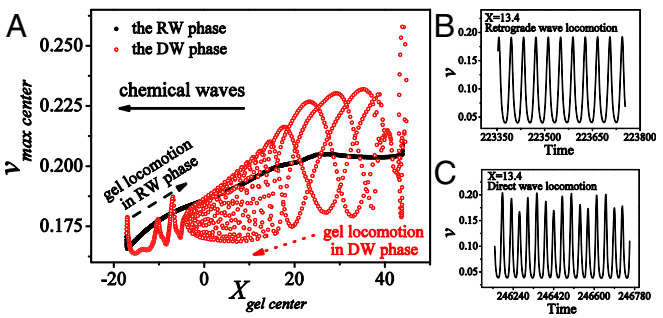


**Fig. 5.** $v_{maxcenter}$ vs. $X_{gelcenter}$ and local oscillations from RW to DW locomotion. (*A*) $v_{maxcenter}$ vs. $X_{gelcenter}$. The black solid and red open circles denote the trajectories in the RW and the DW phases, respectively. The black dashed and red dotted arrows indicate the locomotion direction of the gel center in the two phases. *B* and *C* show time series of $v$ at $X_{gelcenter}$ = 13.4 for the RW and DW locomotion, respectively.

example is in Movie S2). A group of these would be analogous to a school of migrating fish or a flock of birds.

Similarly, animals, such as salmon, eel, gnu, reptiles, and birds, migrate along gradients of environmental parameters (e.g., food species, temperature, and light intensity). Different migration areas induce specific functions (e.g., young salmon grow in the sea, and mature salmon spawn in the fresh water of small rocky tributaries). How does this periodic migration occur? We may speculate that environmental variation induces different nerve pulse structures, similar to the changes between Fig. 1 *E* and *F* in the chemical system, resulting in reversal of the net direction of locomotion (i.e., reciprocating migration).

Autonomous reciprocating migration of active matter not only plays an essential role in the ecological balance and cycles of matter but may also have applications in devices and machines [for example, to design molecular machines (35) or soft robots (36) with better adaptation to the environment]. In uncontrollable environments with extreme or delicate conditions, devices capable of autonomous reciprocating motion to execute a task and then return for periodic duty would have considerable advantages. A potential medical application would consist of a drug delivery system for delicate veins (37), in which micro-/nanorobots in the blood move along a concentration gradient of oxygen (or other species) to access the nidus, release drugs, and then return to the blood for a new round of transport. Another attractive application is to devise an environmental sampling and/or disaster-fighting system for use under severe conditions (e.g., deep sea or nuclear disaster locations), where ordinary robots fail because of high pressure or nuclear radiation. Such a specifically designed soft robot would sense its objective and return safely after performing its function.

Finally, we note that the pattern of illumination used here consists of a single 1D linear ramp, which results in simple back and forth motion. Our results suggest that more complex patterns of illumination, particularly in two spatial dimensions, could be designed to generate quite intricate trajectories of gel motion.

## Methods

Our model couples the Yashin–Balazs gel model (22–24) with the photosensitive Oregonator model of Amemiya et al. (29) in its two-variable form (27). The partial differential equations and computational details are given in *SI Text*. The BZ gel is idealized to be confined within a pseudo-1D capillary tube, where only one direction of gel swelling is unrestricted. Our dimensionless unit of length corresponds to 0.04 mm. The light intensity along the *x* axis is shown in Fig. S2, where there are three illuminated regions. The left and right parts of the capillary tube are in the darker and brighter illumination regions, respectively. The central part is a transition region, in which there is a linear increase of light intensity. The light intensities in the two end regions are denoted $I_{left}$ and $I_{right}$. The length of the transition region is $L_{transiton}$, and the apparent angle between the horizontal $I_{left}$ line and the diagonal $L_{transiton}$ line is $\alpha$. The location and light intensities of the illuminated regions are maintained throughout each simulation. In all scenarios, we initially add random noise to the values of *u* and *v* with an amplitude of 5% of their steady-state values.

**ACKNOWLEDGMENTS.** We thank Dr. V. V. Yashin for help with the gLSM. This work was supported by Grant 21573282 from the National Natural Science Foundation of China, Fundamental Research Funds for the Central Universities Grant 2015XKZD09, the Priority Academic Program Development of Jiangsu Higher Education (PAPD), the W. M. Keck Foundation, and US National Science Foundation Grant CHE-1362477.

1. Gonzalez-Rodriguez D, Guevorkian K, Douezan S, Brochard-Wyart F (2012) Soft matter models of developing tissues and tumors. *Science* 338:910–917.
2. Ramaswamy S (2010) The mechanics and statistics of active matter. *Annu Rev Condens Matter Phys* 1:323–345.
3. Marchetti MC, et al. (2013) Hydrodynamics of soft active matter. *Rev Mod Phys* 85: 1143–1189.
4. Vicsek T, Zafeiris A (2012) Collective motion. *Phys Rep* 517:71–140.
5. Azam F (1998) Microbial control of oceanic carbon flux: The plot thickens. *Science* 280: 694–696.
6. Jékely G (2009) Evolution of phototaxis. *Philos Trans R Soc Lond B Biol Sci* 364: 2795–2808.
7. Cluzel P, Surette M, Leibler S (2000) An ultrasensitive bacterial motor revealed by monitoring signaling proteins in single cells. *Science* 287:1652–1655.
8. Dusenbery DB (2009) *Living at Micro Scale: The Unexpected Physics of Being Small* (Harvard Univ Press, Cambridge, MA).
9. Stocker R (2012) Marine microbes see a sea of gradients. *Science* 338:628–633.
10. Zhang J, Guo W-H, Wang Y-L (2014) Microtubules stabilize cell polarity by localizing rear signals. *Proc Natl Acad Sci USA* 111:16383–16388.
11. Béguer-Pon M, Castonguay M, Shan S, Benchetrit J, Dodson JJ (2015) Direct observations of American eels migrating across the continental shelf to the Sargasso Sea. *Nat Commun* 6:8705.
12. Hoare B (2009) *Animal Migration: Remarkable Journeys in the Wild* (Univ of California Press, Berkeley, CA).
13. Aidley DJ (1981) *Animal Migration* (Cambridge Univ Press, Cambridge, UK).
14. Fraley SI, Feng Y, Giri A, Longmore GD, Wirtz D (2012) Dimensional and temporal controls of three-dimensional cell migration by zyxin and binding partners. *Nat Commun* 3:719.
15. Camley BA, Zhao Y, Li B, Levine H, Rappel WJ (2013) Periodic migration in a physical model of cells on micropatterns. *Phys Rev Lett* 111:158102.
16. Lin YT, et al. (2015) Pulled polymer loops as a model for the alignment of meiotic chromosomes. *Phys Rev Lett* 115:208102.
17. Paoluzzi M, Di Leonardo R, Angelani L (2015) Self-sustained density oscillations of swimming bacteria confined in microchambers. *Phys Rev Lett* 115:188303.
18. Zaikin AN, Zhabotinsky AM (1970) Concentration wave propagation in two-dimensional liquid-phase self-oscillating system. *Nature* 225:535–537.
19. Yoshida R, Takahashi T, Yamaguchi T, Ichijo H (1996) Self-oscillating gel. *J Am Chem Soc* 118:5134–5135.
20. Maeda S, Hara Y, Sakai T, Yoshida R, Hashimoto S (2007) Self-walking gel. *Adv Mater* 19:3480–3484.
21. Ren L, et al. (2016) Retrograde and direct wave locomotion in a photosensitive self-oscillating gel. *Angew Chem Int Ed Engl* 55:14301–14305.
22. Yashin VV, Balazs AC (2006) Modeling polymer gels exhibiting self-oscillations due to the Belousov–Zhabotinsky reaction. *Macromolecules* 39:2024–2026.
23. Yashin VV, Balazs AC (2007) Theoretical and computational modeling of self-oscillating polymer gels. *J Chem Phys* 126:124707.
24. Kuksenok O, Yashin VV, Balazs AC (2008) Three-dimensional model for chemo-responsive polymer gels undergoing the Belousov-Zhabotinsky reaction. *Phys Rev E Stat Nonlin Soft Matter Phys* 78:041406.
25. Yashin VV, Balazs AC (2006) Pattern formation and shape changes in self-oscillating polymer gels. *Science* 314:798–801.
26. Shinohara S, Seki T, Sakai T, Yoshida R, Takeoka Y (2008) Photoregulated wormlike motion of a gel. *Angew Chem Int Ed Engl* 47:9039–9043.
27. Lu X, et al. (2013) Photophobic and phototropic movement of a self-oscillating gel. *Chem Commun (Camb)* 49:7690–7692.
28. Ijspeert AJ (2014) Biorobotics: Using robots to emulate and investigate agile locomotion. *Science* 346:196–203.
29. Amemiya T, Ohmori T, Nakaiwa M, Yamaguchi T (1998) Two-parameter stochastic resonance in a model of the photosensitive Belousov–Zhabotinsky reaction in a flow system. *J Phys Chem A* 102:4537–4542.
30. Ren L, et al. (2015) Experimental, numerical, and mechanistic analysis of the non-monotonic relationship between oscillatory frequency and photointensity for the photosensitive Belousov-Zhabotinsky oscillator. *Chaos* 25:064607.
31. Mikhailov AS, Engel A (1986) Multiple target pattern creation and synchronization phenomena. *Phys Lett A* 117:257–260.
32. Blasius B, Tönjes R (2005) Quasiregular concentric waves in heterogeneous lattices of coupled oscillators. *Phys Rev Lett* 95:084101.
33. Kheowan O-U, Mihaliuk E, Blasius B, Sendiña-Nadal I, Showalter K (2007) Wave mediated synchronization of nonuniform oscillatory media. *Phys Rev Lett* 98:074101.
34. Bär M, et al. (1994) Chemical turbulence and standing waves in a surface reaction model: The influence of global coupling and wave instabilities. *Chaos* 4:499–508.
35. Watson MA, Cockroft SL (2016) Man-made molecular machines: Membrane bound. *Chem Soc Rev* 45:6118–6129.
36. Wehner M, et al. (2016) An integrated design and fabrication strategy for entirely soft, autonomous robots. *Nature* 536:451–455.
37. Li J, Mooney DJ (2016) Designing hydrogels for controlled drug delivery. *Nat Rev Mater* 1:16071.